applied sciences

MDPI

Article

Examining Interactions of Uranyl(VI) Ions with Amino Acids in the Gas Phase

Ana F. Lucena [1,†], Leonor Maria [1], John K. Gibson [2] and Joaquim Marçalo [1,*]

[1] Centro de Química Estrutural, Institute of Molecular Sciences, Instituto Superior Técnico, Universidade de Lisboa, 2695-066 Bobadela, Portugal
[2] Chemical Sciences Division, Lawrence Berkeley National Laboratory, Berkeley, CA 94720, USA
* Correspondence: jmarcalo@ctn.tecnico.ulisboa.pt
† Current address: Reference Materials Unit, Joint Research Centre, European Commission, 2440 Geel, Belgium.

Abstract: Gas-phase experiments, using electrospray ionization quadrupole ion trap mass spectrometry (ESI-QIT/MS), were conducted to probe basic interactions of the uranyl(VI) ion, UO_2^{2+}, with selected natural amino acids, namely, L-cysteine (Cys), L-histidine (His), and L-aspartic acid (Asp), which strongly bind to metal ions. The simplest amino acid, glycine (Gly), was also studied for comparison. Cys, His, and Asp have additional potentially coordinating groups beyond the amino and carboxylic acid functional groups, specifically thiol in Cys, imidazole in His, and a second carboxylate in Asp. Gas-phase experiments comprised collision-induced dissociation (CID) of uranyl–amino acid complexes and competitive CID to assess the relative binding strength of different amino acids in the same uranyl complex. Reactivity of selected uranyl–amino acid complexes with water provided further insights into relative stabilities. In positive ion mode, CID and ensuing reactions with water suggested that uranyl–neutral AA binding strength decreased in the order His > Asp > Cys > Gly, which is similar to amino acid proton affinities. In negative ion mode, CID revealed a decreasing dissociation tendency in the order Gly >> His ≈ Cys > Asp, presumably reflecting a reverse enhanced binding to uranyl of the doubly deprotonated amino acids formed in CID.

Keywords: uranyl ions; amino acids; gas-phase ion chemistry; electrospray ionization mass spectrometry

Citation: Lucena, A.F.; Maria, L.; Gibson, J.K.; Marçalo, J. Examining Interactions of Uranyl(VI) Ions with Amino Acids in the Gas Phase. *Appl. Sci.* **2023**, *13*, 3834. https://doi.org/10.3390/app13063834

Academic Editor: Claudio Medana

Received: 27 February 2023
Revised: 11 March 2023
Accepted: 15 March 2023
Published: 17 March 2023

1. Introduction

The extensive use of uranium and other actinides in nuclear technology introduces the possibility of contamination that may induce both radiological and chemical toxicity [1]. Uranium has no role in normal biochemical processes in living organisms, but understanding its interactions with biomolecules, such as proteins, is key to illuminating its high toxicity and elaborating toxicological models [2–9].

The most stable form of uranium under biological conditions is the uranyl(VI) ion, UO_2^{2+}. It can develop strong interactions with biomolecules due to its physicochemical properties, and it has the ability to replace essential divalent metal ions, which may result in significant disruption to their natural functions. Following a contamination event, biological fluids will transport absorbed uranyl toward different organs through binding to particular biomolecules.

Many studies have been performed to understand the interactions between uranium and biomolecules, including amino acids and peptides as protein building blocks, but better comprehension of structure–function relationships is still needed [10–13]. Such knowledge is key to assessing mechanisms of uranium toxicity and developing new molecules for selective uranyl binding in decorporation and bioremediation [14–17]. Such insight is also useful for the development of sensitive and selective peptide/protein-based uranyl sensors for environmental detection and remediation [18–23].

Gas-phase studies based on mass spectrometry (MS) can provide intrinsic physical and chemical properties of elementary species and can elucidate relationships between molecular and electronic structure, energetics, and reactivity. MS, often accompanied by spectroscopic experiments and theoretical studies, has long been employed in the fundamental investigation of metal–ion interactions with molecules of biological relevance, with emphasis on alkali, alkaline earth, and key transition metals [24–26].

Infrared multiphoton dissociation (IRMPD) spectroscopy is an established approach for obtaining structural and conformational information on gas-phase metal ion complexes, with many recent investigations addressing systems of biochemical relevance [27–30]. Amino acids, the elementary components of peptides and proteins, tend to be zwitterions in an aqueous solution, while the more even charge distribution is more stable in the gas phase. However, the charge distribution may change upon coordination to a metal ion, with competition between zwitterion/salt bridge (SB) and charge solvation (CS) modes of complexation. For deprotonated amino acids, a main consideration is the site of deprotonation, which is clearly the carboxylic acid terminus in solution but may be different in the gas phase. IRMPD studies have contributed to unraveling these issues for various metal ions.

The approaches noted above have not yet been used to examine interactions of uranyl with simple biomolecules. Therefore, the study of gas-phase interactions of uranyl(VI) with selected natural amino acids using ESI-MS and tandem MS appeared significant, this serving as preliminary scrutiny to lay the groundwork for more elaborate spectroscopic and computational studies.

2. Materials and Methods

2.1. Materials

Natural or depleted uranium compounds used in this work comprise alpha-emitting radionuclides, ^{238}U ($t_{1/2}$ = 4.468 × 10^9 years, α-particle energy 4.27 MeV), ^{235}U ($t_{1/2}$ = 7.04 × 10^8 years, α-particle energy 4.68 MeV), and ^{234}U ($t_{1/2}$ = 2.46 × 10^5 years, α-particle energy 4.86 MeV) [31]; ^{238}U is the primary component of uranium, both natural (~99.3% ^{238}U) and depleted (~99.8% ^{238}U). Adequate radiological safety precautions were taken in all experiments.

Uranyl/amino acid solutions were prepared from 1–4 vol. of 1 mM amino acid solutions in H_2O (glycine, L-histidine, L-cysteine, L-aspartic acid; commercial products with >99.9% purity), plus 1 vol. of 1 mM solution in H_2O of $UO_2Cl_2(H_2O)_n$ (commercial product with >99.9% purity). Uranyl/amino acid mixtures were diluted in 2–5 vol. of ethanol to enhance ESI-MS performance. The pH of the solutions was in the range 5–7, with cysteine solutions being generally the most acidic. Cysteine solutions needed to be freshly prepared because cystine is easily formed by condensation of two cysteine molecules covalently linked via a disulfide bond. For competitive CID experiments, H_2O solutions with two different amino acids were prepared with a 1:1 stoichiometry and then mixed with uranyl chloride solutions in H_2O and diluted with ethanol to yield a concentration of uranyl of ~10^{-4} M, some 2–4 times that of the amino acids.

2.2. Methods

A Bruker HCT quadrupole ion trap mass spectrometer (QIT/MS) equipped with an ESI source was used in all experiments. Mass spectra were recorded in positive and negative ion accumulation and detection modes. Sample solutions were introduced through a nebulizer with a syringe pump at 150 μL h^{-1}. Mass spectra were acquired using the following typical instrumental parameters: nebulizer gas pressure, 8.0 psi; capillary voltage, −/+4000 V; dry gas flow rate, 4.0 L min^{-1}; dry gas temperature, 250 °C; capillary exit, +/−128.5 V; skimmer, +/−40.0 V. Nitrogen gas from a nitrogen generator was used for nebulization and drying in the ion transfer capillary. The helium buffer-gas pressure in the ion trap was constant at ~1 × 10^{-4} Torr, and the background water and oxygen pressures were estimated to be ~10^{-6} Torr each. The MS^n capabilities of the QIT were used for the

isolation of ions with a specific m/z, for subsequent collision-induced dissociation (CID) experiments with mass-selected ions using the helium buffer gas as collision partner, or for introducing an ion/molecule reaction time of up to 10 s without ion excitation. The helium provides third-body collisions, which remove energy and stabilize product ions after CID, as well as thermalizing reagent ions and stabilizing product ions in ion/molecule reactions. Pseudo-first-order rates, k, for thermal (~300 K) reactions of trapped ions in the QIT were obtained by isolating the ion of interest and allowing it to react with background water or oxygen for variable times. When reaction products efficiently formed during CID experiments and rendered reagent ion isolation impractical, rough estimates of reaction rates were inferred from relative abundances of reagent and product ions in CID spectra, considering the CID timescale of ~40 ms.

3. Results and Discussion

3.1. ESI-MS of Uranyl Complexes with Glycine, Aspartic Acid, Cysteine, and Histidine

ESI-MS of mixtures of uranyl(VI) chloride and glycine (Gly), aspartic acid (Asp), cysteine (Cys), or histidine (His) in water/ethanol generated monopositive and mononegative complexes containing the UO_2^{2+} ion coordinated by one to three neutral (AA) or deprotonated ($(AA\text{-}H)^-$) amino acids (Scheme S1 shows the structures of studied amino acids). The general formulas of the main complexes obtained are as follows: in the positive ion mode, $[UO_2(AA\text{-}H)(AA)_2]^+$, $[UO_2(AA\text{-}H)(AA)]^+$, $[UO_2(Cl)(AA)_2]^+$, and $[UO_2(Cl)(AA)]^+$; in the negative ion mode, $[UO_2(AA\text{-}H)_3]^-$, $[UO_2(Cl)(AA\text{-}H)_2]^-$, and $[UO_2(Cl)_2(AA\text{-}H)]^-$. Figures 1 and 2 show illustrative spectra for the cases of Cys in positive ion mode and His in negative ion mode, respectively, and Figures S1–S6 present spectra for the remaining cases in both ion modes. Tables S1 and S2 summarize the main results of ESI-MS in positive and negative ion modes, respectively, including m/z assignments.

In some cases, in the positive ion mode, water-addition products were also observed (see Figures 1 and S1–S3). As precursor $[UO_2(AA\text{-}H)(AA)]^+$ complexes were also present in the spectra, water-addition products were considered water adducts and not complexes with one hydroxide and two neutral AAs. Furthermore, simple water addition can prevail as the gas-phase acidity of H_2O is 200–280 kJ mol^{-1} larger than that of the AA (see Table S3 for a compilation of gas-phase data for the studied amino acids [32]; the gas-phase acidity of water is 1633 kJ mol^{-1} [33]); this could compensate differences in relative binding strengths of OH^- vs. $(AA\text{-}H)^-$ and H_2O vs. AA to uranyl (there are no available data for this evaluation).

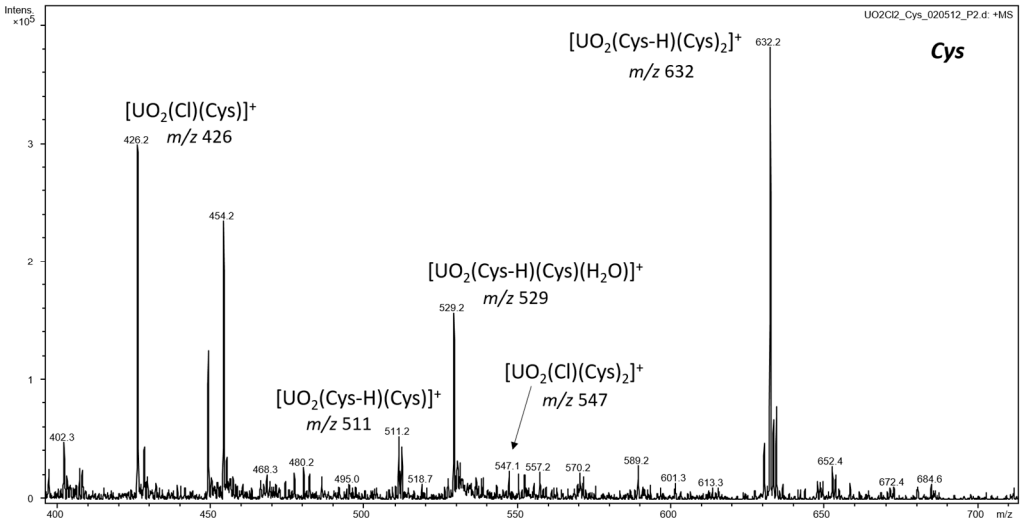

Figure 1. ESI-MS of a uranyl chloride + cysteine solution (1:4) in positive ion mode.

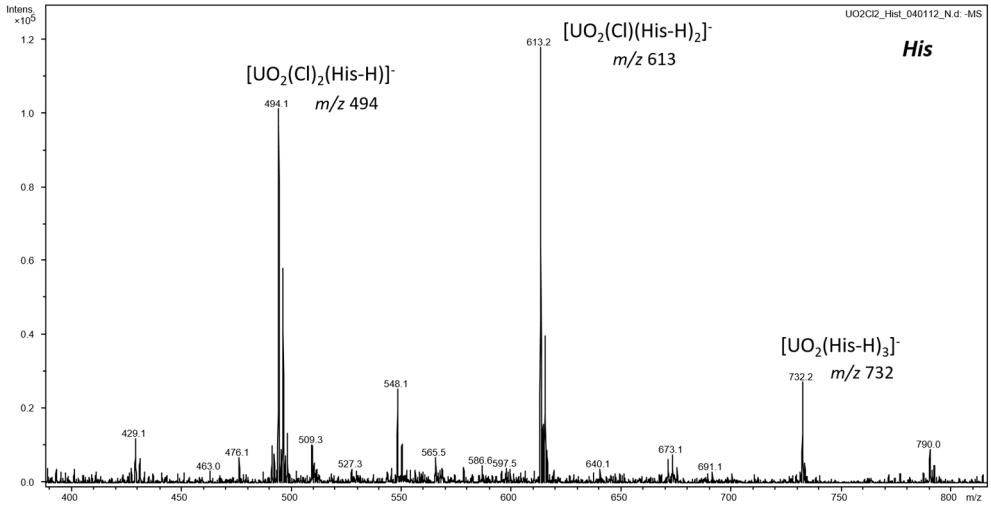

Figure 2. ESI-MS of a uranyl chloride + histidine solution (1:4) in negative ion mode.

Uranyl complexes containing cystine (Cis) were identified in spectra obtained from UO_2Cl_2+Cys solutions, as cystine easily forms through condensation of two cysteine molecules that covalently link via a disulfide bond (see Figure S6; see also Scheme S2 that shows the structure of cystine).

Comprising a soft ionization method, ESI-MS may directly reveal solution speciation of metal complexes. However, due to the intrinsically complex mechanism of electrospray, as well as perturbations during ion transfer from ambient to low pressures, and other factors, gas-phase species from ESI do not necessarily directly represent those in solution [34–37]. As the focus is on gas-phase uranyl–amino acid complexes, the issue of solution speciation was mostly sidestepped.

It is notable that in negative ion mode the relative abundance of $[UO_2(AA\text{-}H)_3]^-$ for the four different amino acids parallels their gas-phase acidities [32]. The most acidic, aspartic acid, displays $[UO_2(Asp\text{-}H)_3]^-$ as the base peak in the spectrum, whereas the least acidic, glycine, shows only minor $[UO_2(Gly\text{-}H)_3]^-$; cysteine and histidine are intermediate (see Figures 2 and S4–S6, and also Table S3).

Gas- and condensed-phase properties are frequently dissimilar, with the acidity of amino acids being no exception as solution pK_a [38] indicates histidine as the most acidic, glycine again as the least acidic, and aspartic acid and cysteine as intermediate (see Figures 2 and S4–S6; Table S4 compiles solution data for the amino acids).

Uranyl(VI), the linear U(VI) dioxido cation UO_2^{2+}, coordinates ligands in the equatorial plane with typical coordination numbers between 3 and 6, depending on ligand size, denticity, and binding strength. The main cationic and anionic uranyl complexes identified here suggest equatorial coordination number 3 in $[UO_2(Cl)(AA)]^+$, 4 in $[UO_2(AA\text{-}H)(AA)]^+$ and $[UO_2(Cl)_2(AA\text{-}H)]^-$, 5 in $[UO_2(Cl)(AA)_2]^+$ and $[UO_2(Cl)(AA\text{-}H)_2]^-$, and 6 in $[UO_2(AA\text{-}H)(AA)_2]^+$ and $[UO_2(AA\text{-}H)_3]^-$. Coordination of the amino acids to "oxophilic" uranyl is implicitly assumed to be through both oxygen atoms of carboxyl for neutral AAs or carboxylate for deprotonated AAs. Scheme 1 shows possible structures for the mentioned complexes where zwitterionic forms of neutral AAs are presumed.

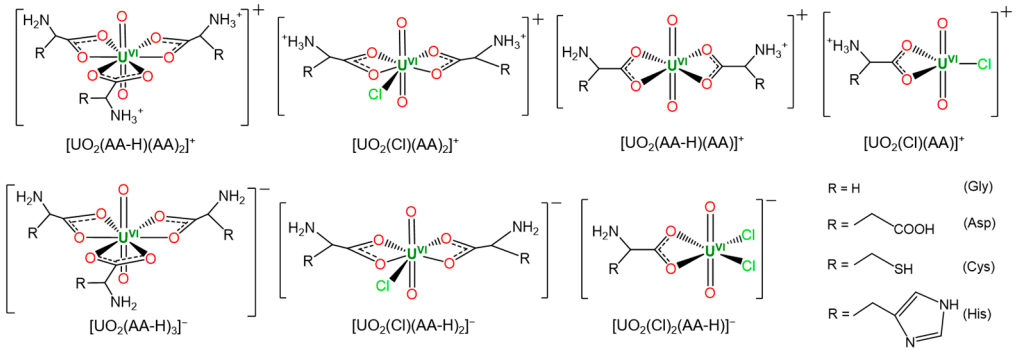

Scheme 1. Conceivable structures for cationic and anionic uranyl–amino acid complexes.

Gas-phase anionic uranyl–carboxylate complexes $[UO_2(RCO_2)_3]^-$ (R = Me, Ph) were studied by Groenewold et al. using MS coupled to IRMPD spectroscopy, complemented by DFT computations [39]. The IRMPD results indicated that the complexes comprised two bidentate carboxylates and one monodentate carboxylate, while DFT pointed to two energetically indistinguishable conformers, with either two bidentate and one monodentate or three bidentate carboxylates.

In contrast to simple carboxylates, the amino group in amino acids, as well as the sidechain functionalities of cysteine (thiol), histidine (imidazole), and aspartic acid (additional carboxyl), can coordinate to uranyl. Insight into the actual uranyl coordination was searched for with MS^n experiments described below.

3.2. CID and Reactivity of Uranyl–Glycine, Uranyl–Aspartic Acid, Uranyl–Cysteine, and Uranyl–Histidine Complexes

Collision-induced dissociation (CID) experiments using the helium buffer gas as a collision partner were performed for dominant cationic and anionic uranyl–amino acid complexes. Also reported here are results for some reactions of complexes with water or oxygen present in the ion trap as background gases.

3.2.1. Cationic Uranyl–Amino Acid Complexes

The main cationic uranyl–amino acid complexes identified were $[UO_2(AA\text{-}H)(AA)_2]^+$ and $[UO_2(Cl)(AA)_2]^+$; $[UO_2(AA\text{-}H)(AA)]^+$ and $[UO_2(Cl)(AA)]^+$ were minor species not examined by CID. Table 1 summarizes the CID results in positive ion mode.

Table 1. CID of cationic uranyl–amino acid complexes.

Precursor Complex	Neutral Losses (%)			
	Gly	Asp	Cys	His
$[UO_2(Cl)(AA)_2]^+$	-HCl (50) -HCl-CO_2 (50)	-HCl (100)	-HCl (50) -HCl-NH_3 (50)	-HCl (100)
$[UO_2(AA\text{-}H)(AA)_2]^+$	-AA (50) -AA-CO_2 (50)	-CO_2 (10) -AA (75) -AA-CO_2 (15)	-NH_3 (55) -AA (25) -AA-NH_3 (20)	-AA (100)

For all four amino acids, CID of $[UO_2(AA\text{-}H)(AA)_2]^+$ led to the elimination of a neutral amino acid followed by immediate water addition on the ~40 ms CID timescale, forming $[UO_2(AA\text{-}H)(AA)(H_2O)]^+$ for all AAs except His. Figure 3 shows a representative mass spectrum for the case of $[UO_2(Gly\text{-}H)(Gly)_2]^+$, while Figures S7–S9 present spectra for the other amino acids. Additional observed fragmentation channels were CO_2-loss for the Gly and Asp complexes and NH_3-loss for the Cys complex.

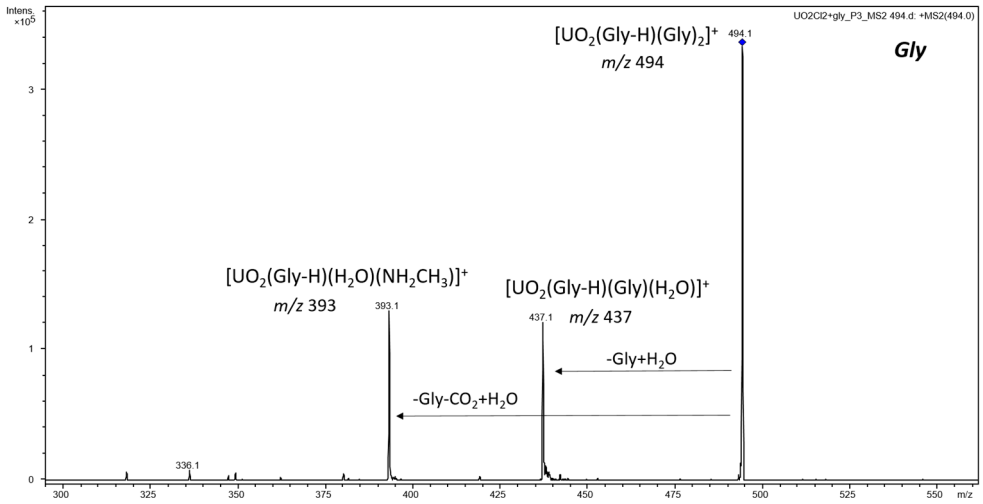

Figure 3. CID mass spectrum of $[UO_2(Gly\text{-}H)(Gly)_2]^+$.

CID of all $[UO_2(Cl)(AA)_2]^+$ except the His case led to the elimination of HCl with the immediate formation of $[UO_2(AA\text{-}H)(AA)(H_2O)]^+$. These were again, as commented above, considered water adducts and not complexes with hydroxide and two neutral AAs. Figure 4 shows the CID mass spectrum of $[UO_2(Gly\text{-}H)(Gly)_2]^+$, while Figures S10–S12 present spectra for the remaining cases. Additional fragmentation channels were CO_2-loss for the Gly complex and NH_3-loss for the Cys complex.

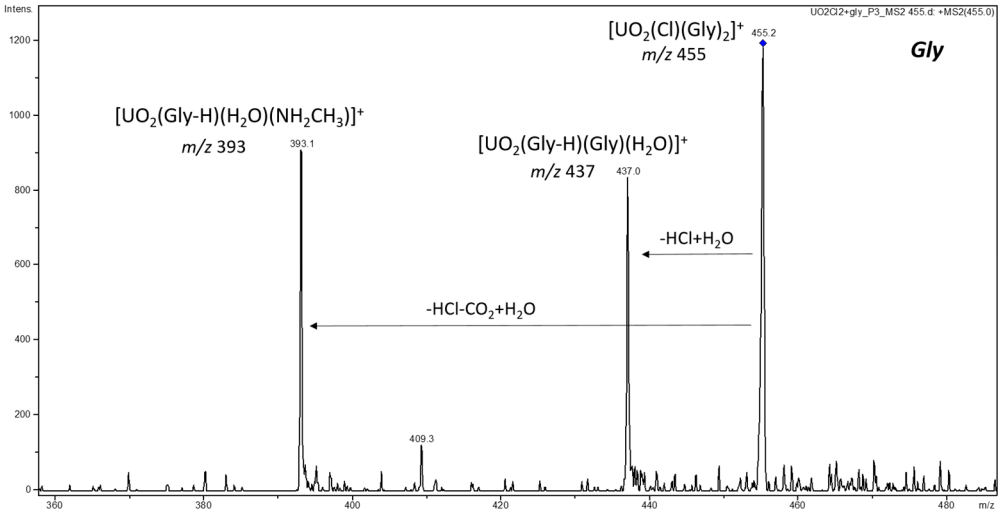

Figure 4. CID mass spectrum of $[UO_2(Cl)(Gly)_2]^+$.

For uncoordinated protonated amino acids, loss of NH_3 is typical of sulfur-containing ones such as cysteine, and loss of H_2O+CO is prevalent for most others [40–43]. Under the present experimental conditions, these were also the main fragmentations observed for protonated Gly, Asp, Cys, and His (see Figures S13–S16 in the SI). Loss of CO_2 (decarboxylation) is a common feature of gas-phase metal complexes with carboxylate ligands [44], and studies with such uranyl complexes have shown decarboxylation as an effective route to remarkable uranyl species [45–47].

Formation of $[UO_2(AA\text{-}H)(AA)(H_2O)]^+$ by prompt hydration of $[UO_2(AA\text{-}H)(AA)]^+$ for AA = Gly, Asp, and Cys, but not His, was compared through estimates of the reaction rates: k[Gly] ≈ k[Cys] (very fast, >70 s^{-1}) > k[Asp] (fast, ~10 s^{-1}) >> k[His] (no reaction up to 10 s). This comparison suggests that the $[UO_2(AA\text{-}H)(AA)]^+$ complexes are undercoordinated for Gly, Asp, and Cys, but not for His, possibly pointing to an important role for the imidazole sidechain group of histidine in coordinating uranyl.

3.2.2. Anionic Uranyl–Amino Acid Complexes

The main identified anionic uranyl–amino acid complexes, $[UO_2(AA\text{-}H)_3]^-$, $[UO_2(Cl)(AA\text{-}H)_2]^-$, and $[UO_2(Cl)_2(AA\text{-}H)]^-$, were examined by CID. Table 2 summarizes the CID results in negative ion mode.

Table 2. CID of anionic uranyl–amino acid complexes.

Precursor Complex	Neutral Losses (%)			
	Gly	Asp	Cys	His
$[UO_2(Cl)_2(AA\text{-}H)]^-$	-(AA-H) (55) $-CO_2$ (45)	-HCl (100)	-HCl (100)	-HCl (100)
$[UO_2(Cl)(AA\text{-}H)_2]^-$	-(AA-H) (100)	-HCl (100)	-HCl (100)	-AA (25) -HCl (75)
$[UO_2(AA\text{-}H)_3]^-$	-(AA-H) (100)	-AA (100)	-AA (100)	-AA (100)

Fragmentation of $[UO_2(AA\text{-}H)_3]^-$ led to the elimination of a neutral amino acid for Asp, Cys, and His, yielding $[UO_2(AA\text{-}2H)(AA\text{-}H)]^-$ (see Figures S17–S19), which presumably contain a doubly deprotonated AA and conserve the +VI oxidation state of uranium. In contrast, CID of $[UO_2(Gly\text{-}H)_3]^-$ did not show the elimination of Gly but instead showed the elimination of (Gly-H), generating uranyl(V) in $[UO_2(Gly\text{-}H)_2]^-$, as shown in Figure 5. This distinctive behavior of the Gly complex likely reflects the absence of a sidechain group in Gly. In accord with gas-phase CID, solution acidities of amino acids (see Table S4) show higher acidities of sidechain groups (pK_c) versus amino groups (pK_b) for Asp, Cys, and His.

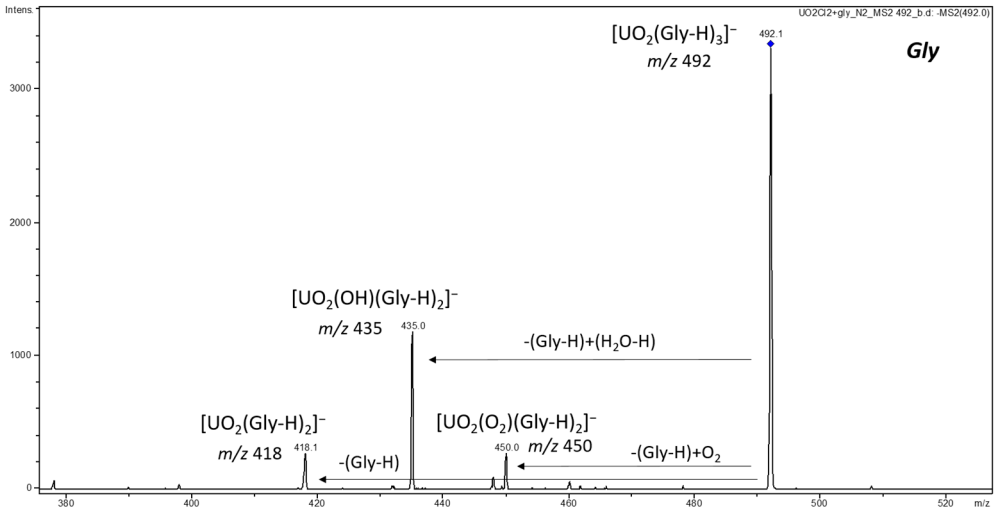

Figure 5. CID mass spectrum of $[UO_2(Gly\text{-}H)_3]^-$.

The formation of a uranyl(V)-Gly complex is substantiated by the formation of an O_2-addition product, $[UO_2(O_2)(Gly\text{-}H)_2]^-$, from reaction with background O_2 on the timescale of CID, a result analogous to O_2 addition previously observed for other anionic uranyl(V) complexes [48].

The reaction of O_2 with cationic and anionic uranyl(V) complexes to yield uranyl(VI) superoxides is well known [49–52]. The rate of O_2 addition to $[UO_2(Gly\text{-}H)_2]^-$ was measured as $k = 15\ s^{-1}$, which is comparable to rates previously reported under similar conditions for $[U^VO_2(X)_2]^-$ complexes comprising bidentate ligands [48]. The $[U^VO_2(Gly\text{-}H)_2]^-$ complex was also prone to hydrolysis by background water to form $[U^{VI}O_2(OH)(Gly\text{-}H)_2]^-$, a phenomenon previously reported for other uranyl(V) complexes [52].

Interestingly, CID product $[UO_2(His\text{-}2H)(His\text{-}H)]^-$ reacted quickly with background water to produce $[UO_2(OH)(His\text{-}H)_2]^-$ during the experiment, while no such hydrolysis was observed for Asp and Cys complexes (see Figures S17–S19). Reactions of $[UO_2(AA\text{-}2H)(AA\text{-}H)]^-$ complexes with water are supposed to yield $[UO_2(OH)(AA\text{-}H)_2]^-$ and not $[UO_2(AA\text{-}2H)(AA\text{-}H)(H_2O)]^-$ as the second removed proton is clearly less acidic than the first; although there are no gas-phase data to substantiate this assumption, solution data may provide this indication (see pK_a and pK_c in Table S4).

Estimated reaction rates with water, k[His] (fast, ~11 s^{-1}) >> k[Asp] ≈ k[Cys] (no reaction up to 10 s), may suggest that the binding strength of doubly deprotonated ligands to uranyl is lower for histidine versus aspartic acid or cysteine. These differences in rates may as well reflect kinetic barriers due to differences in coordination of the doubly deprotonated amino acids.

CID of $[UO_2(Cl)(AA\text{-}H)_2]^-$ led to the elimination of HCl for Asp, Cys, and His, again yielding $[UO_2(AA\text{-}2H)(AA\text{-}H)]^-$ (see Figures S20–S22). Once more, $[UO_2(His\text{-}2H)(His\text{-}H)]^-$ reacted rapidly with background water to produce $[UO_2(OH)(His\text{-}H)_2]^-$, while no reaction (up to 10 s) was observed for the Asp and Cys complexes. Intriguingly, CID of $[UO_2(Cl)(His\text{-}H)_2]^-$ also led to the elimination of His, concurrent with prompt reaction with water to give $[UO_2(Cl)(OH)(His\text{-}H)]^-$, suggesting weaker binding of deprotonated histidine to uranyl compared to deprotonated aspartic acid or cysteine.

CID of $[UO_2(Cl)(Gly\text{-}H)_2]^-$ was dissimilar to the corresponding complexes comprising the other amino acids, but in accord with results for $[UO_2(Gly\text{-}H)_3]^-$, as shown in Figure 6. Loss of (Gly-H) was the only observed fragmentation, forming a new uranyl(V) complex, $[UO_2(Cl)(Gly\text{-}H)]^-$, which reacted with O_2 to yield $[UO_2(Cl)(O_2)(Gly\text{-}H)]^-$ and H_2O to produce $[UO_2(Cl)(OH)(Gly\text{-}H)]^-$. The rate of O_2 addition to $[UO_2(Cl)(Gly\text{-}H)]^-$ (k = 11 s^{-1}) was slightly lower than that above for $[UO_2(Gly\text{-}H)_2]^-$ (k = 15 s^{-1}).

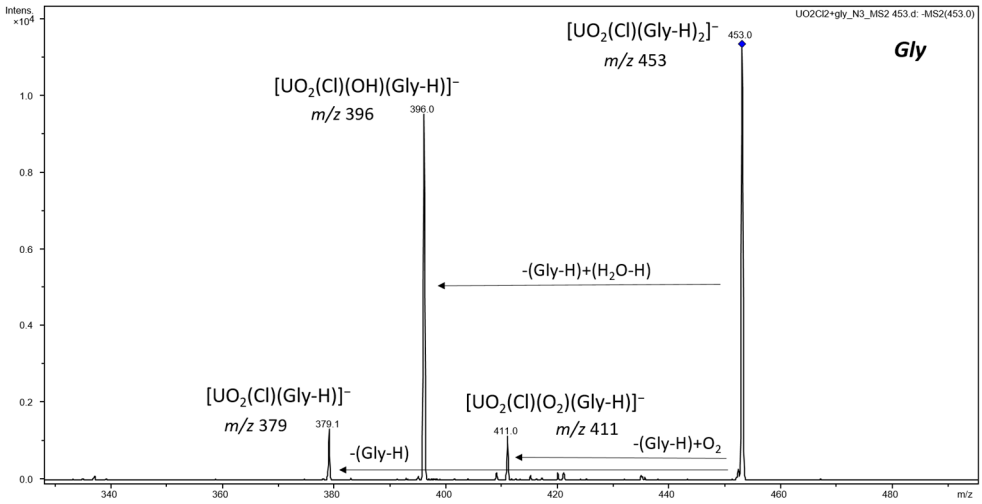

Figure 6. CID mass spectrum of $[UO_2(Cl)(Gly\text{-}H)_2]^-$.

CID of $[UO_2(Cl)_2(AA\text{-}H)]^-$ mainly eliminated HCl for Asp, Cys, and His, forming $[UO_2(AA\text{-}2H)(Cl)]^-$ (see Figures S23–S25), which reacted with background water to give $[UO_2(Cl)(OH)(AA\text{-}H)]^-$ with very different rates: k[His] (very fast, >70 s^{-1}) > k[Cys] (fast, ~36 s^{-1}) >> k[Asp] (slow, ~1 s^{-1}). Loss of (AA-H) followed by prompt hydrolysis to form $[UO_2(Cl)_2(OH)]^-$ was observed for all three complexes, but was clearly more dominant for the His complex.

As observed in Figure 7, CID of $[UO_2(Cl)_2(Gly\text{-}H)]^-$ eliminated (Gly-H) to form a uranyl(V) species, $[UO_2(Cl)_2]^-$, which hydrolyzed to give $[UO_2(Cl)_2(OH)]^-$. In contrast to the other uranyl(V) complexes discussed above, reaction with background O_2 was not observed, in accord with previous results showing inefficient O_2 addition to $[UO_2(Cl)_2]^-$ [48].

Another important fragmentation channel for $[UO_2(Cl)_2(Gly\text{-}H)]^-$ was decarboxylation to yield $[UO_2(Cl)_2(NHCH_3)]^-$, which presumably comprises a methylamide.

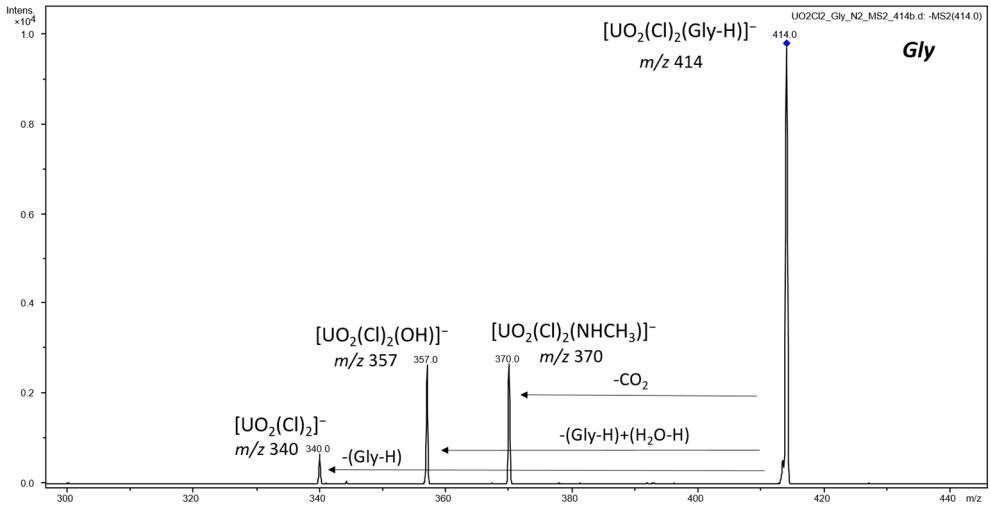

Figure 7. CID mass spectrum of $[UO_2(Cl)_2(Gly\text{-}H)]^-$.

3.3. ESI-MS, Competitive CID, and Reactivity of Mixed Glycine, Aspartic Acid, Cysteine, and Histidine Complexes with Uranyl

ESI-MS complexes comprising two or three amino acids—i.e., cationic $[UO_2(AA\text{-}H)(AA)_2]^+$ and $[UO_2(Cl)(AA)_2]^+$ and anionic $[UO_2(AA\text{-}H)_3]^-$ and $[UO_2(Cl)(AA\text{-}H)_2]^-$—open up the possibility of mixed amino acid complexes that can be examined by CID to assess relative ligand affinities. Such complexes were prepared (see Figures S26–S37) using solutions with two amino acids (AA and AA′) in a 1:1 ratio; signal intensities were predictably lower than those for ESI-MS of solutions with only one amino acid.

In positive ion mode, CID of complexes with one chloride and amino acids AA and AA′, $[UO_2(Cl)(AA)(AA')]^+$, is expected to result in the elimination of HCl, as observed for $[UO_2(Cl)(AA)_2]^+$; as such processes would not be particularly illuminating, CID experiments were not pursued. Two combinations are possible for complexes comprising one deprotonated amino acid and two neutral amino acids: $[UO_2(AA\text{-}H)(AA)(AA')]^+$ and $[UO_2(AA'\text{-}H)(AA)_2]^+$. In the absence of laborious computational studies to deduce the most favorable isomers, we initially assume predominant deprotonation of the most acidic amino acid based on gas-phase acidities: GA[Asp] > GA[His] > GA[Cys] > GA[Gly] (see Table S3). However, the CID results may contradict this simple assumption and suggest two isomers.

In negative ion mode, there is no doubt as to the deprotonation site as all the amino acids are deprotonated in $[UO_2(AA\text{-}H)_2(AA'\text{-}H)]^-$, $[UO_2(AA\text{-}H)(AA'\text{-}H)_2]^-$, and $[UO_2(Cl)(AA\text{-}H)(AA'\text{-}H)]^-$.

3.3.1. Competitive CID and Reactivity of Cationic Uranyl Mixed Amino Acid Complexes

Table 3 summarizes the results of competitive CID experiments in positive ion mode.

Table 3. Competitive CID of cationic uranyl–amino acid complexes.

Precursor Complex	Neutral Losses (%)					
	AA/AA′					
	Asp/Gly	Cys/Gly	His/Gly	Asp/Cys	Asp/His	His/Cys
$[UO_2(AA\text{-}H)(AA')_2]^+$	-AA′ (100)	-NH_3 (10) -AA′ (50) -AA′-NH_3 (25) -AA′-NH_3-CO_2 (15)	-AA′ (55) -AA′-CO_2 (45)	-AA′ (100)	-AA (100)	-AA′ (100)
$[UO_2(AA\text{-}H)(AA)(AA')]^+$	-AA′ (85) -AA (15)	-NH_3 (30) -AA (30) -AA′ (20) -AA′-NH_3 (20)	-AA′ (100)	-AA′ (100)	-AA (100)	-AA′ (100)

All mixed complexes involving Gly showed mainly elimination of Gly, together with less important channels, as shown in Figures S38–S40 for $[UO_2(AA\text{-}H)(Gly)_2]^+$ and Figures S41–S43 for $[UO_2(AA\text{-}H)(AA)(Gly)]^+$, where the indicated deprotonation is based on considerations discussed above. Again observed were loss of NH_3 in Cys-containing complexes and loss of CO_2 in a few cases. Interestingly, loss of AA was also detected for Asp and Cys in $[UO_2(AA\text{-}H)(AA)(Gly)]^+$, with the presence of two AA ligands presumably statistically enhancing the probability of this channel.

For the other amino acids, in alternative isomers $[UO_2(AA\text{-}H)(AA)(AA')]^+$ or $[UO_2(AA'\text{-}H)(AA)_2]^+$, only AA or AA′ losses were observed, as shown in Figures S44–S49. A clear pattern resulted, with Cys elimination from Asp/Cys and Cys/His complexes and Asp elimination from Asp/His complexes. Although this result for Asp/His casts doubt on the tentative assumption that the most acidic amino acid is deprotonated, it is possible that ligand rearrangement during CID, from Asp-H to Asp, favors Asp elimination.

The reaction of $[UO_2(AA'\text{-}H)(AA)]^+$ with background water was observed in most cases, with its fast nature precluding comparisons between amino acids. The overall general picture for the mixed complexes indicates preferred fragmentation involving loss of the amino acid with lower proton affinity: PA[Gly] < PA[Cys] < PA[Asp] < PA[His] (see Table S3) [53]. This suggests that PA is a good indicator of the strength of interactions of uranyl cations with neutral amino acids in gas-phase complexes.

3.3.2. Competitive CID and Reactivity of Anionic Uranyl Mixed Amino Acid Complexes

Table 4 summarizes the results of competitive CID experiments in negative ion mode.

Table 4. Competitive CID of anionic uranyl–amino acid complexes.

Precursor Complex	Neutral Losses (%)					
	AA/AA′					
	Asp/Gly	Cys/Gly	His/Gly	Asp/Cys	Asp/His	His/Cys
$[UO_2(Cl)(AA\text{-}H)(AA'\text{-}H)]^-$	-HCl (90) -AA′ (10)	-HCl (45) -AA′ (55)	-HCl (50) -AA′ (50)	-HCl (100)	-HCl (100)	-HCl (100)
$[UO_2(AA\text{-}H)_2(AA'\text{-}H)]^-$	-AA′ (100)	-AA′ (100)	-AA (35) -AA′ (65)	-AA (10) -AA′ (90)	-AA (45) -AA′ (55)	-AA (85) -AA′ (15)
$[UO_2(AA\text{-}H)(AA'\text{-}H)_2]^-$	-AA′ (100)	-AA′ (100)	-AA′ (100)	-AA′ (100)	-AA′ (100)	-AA (15) -AA′ (85)

It was anticipated that complexes with one chloride and two deprotonated amino acids, $[UO_2(Cl)(AA\text{-}H)(AA'\text{-}H)]^-$, could illuminate the relative binding strengths of different AAs to uranyl cations. However, as CID elimination of HCl was dominant, as for $[UO_2(Cl)(AA\text{-}H)_2]^-$, these experiments were not particularly elucidating (see Figures S50–

S55). When Gly-H was present, as in $[UO_2(Cl)(AA\text{-}H)(Gly\text{-}H)]^-$, loss of Gly but not (Gly-H), as in $[UO_2(Cl)(Gly\text{-}H)_2]^-$, was observed, showing altered behavior due to the presence of an amino acid with a sidechain predisposed to deprotonation.

CID of $[UO_2(AA\text{-}H)_2(AA'\text{-}H)]^-$ and $[UO_2(AA\text{-}H)(AA'\text{-}H)_2]^-$ resulted in the loss of a neutral amino acid in all cases (see Figures S56–S67), with an overall decreasing loss trend of Gly >> His ≈ Cys > Asp. This ordering probably reflects the coordination strength of the residual doubly deprotonated amino acid ligand, which evidently increases from Gly, with no sidechain to deprotonate, to Asp, with a rather acidic sidechain.

Reactivity of $[UO_2(AA\text{-}2H)(AA'\text{-}H)]^-$ from CID with background water was in essential accord with the previous observation that only $[UO_2(His\text{-}2H)(His\text{-}H)]^-$ reacted efficiently, to produce $[UO_2(OH)(His\text{-}H)_2]^-$, while no hydrolysis was observed for Asp and Cys complexes. The mixed ligand complex $[UO_2(His\text{-}2H)(Gly\text{-}H)]^-$ also reacted quickly with water (k~15 s^{-1}), whereas the complexes with Asp/His and Cys/His were unreactive, which suggests that the doubly deprotonated amino acids are Asp-2H and Cys-2H.

4. Conclusions

ESI-MS proved to be an efficient method for producing amino acid complexes of uranyl(VI) in the gas phase, with illustrative results presented for glycine, aspartic acid, cysteine, and histidine. CID and water reactivity provided insight into amino acid coordination and relative binding affinities.

In negative ion mode ESI-MS, the comparative intensities of $[UO_2(AA\text{-}H)_3]^-$, $[UO_2(Cl)(AA\text{-}H)_2]^-$, and $[UO_2(Cl)_2(AA\text{-}H)]^-$ apparently correlate with gas-phase acidities of the amino acids. In positive ion mode, relative intensities of $[UO_2(AA\text{-}H)(AA)_2]^+$, $[UO_2(Cl)(AA)_2]^+$, and $[UO_2(Cl)_2(AA)]^+$ did not reveal such a clear trend.

Glycine complexes showed distinctive behavior, with apparent weaker binding attributed to the absence of a sidechain. CID in negative ion mode demonstrated these differences in that dissociation of $[UO_2(AA\text{-}H)_3]^-$ did not yield $[UO_2(AA\text{-}2H)(AA\text{-}H)]^-$. CID of chloride/AA complexes in both ion modes displayed dominant HCl elimination, except for the case of glycine.

Further insight was provided by the reactivity of CID products with background water. A rapid reaction was observed for $[UO_2(AA\text{-}H)(AA)]^+$ yielding $[UO_2(AA\text{-}H)(AA)(H_2O)]^+$ for AA = Gly, Asp, and Cys, but not His. This suggests that $[UO_2(AA\text{-}H)(AA)]^+$ are undercoordinated for Gly, Asp, and Cys, but not His, probably due to uranyl coordination by the imidazole sidechain of histidine. $[UO_2(AA\text{-}2H)(AA\text{-}H)]^-$ produced by CID reacted with water in the rate order His >> Cys ~ Asp, which suggests that the binding strength of doubly deprotonated histidine to uranyl is lower than that for the other amino acids.

Competitive CID of uranyl species with mixed AAs provided additional insights. In positive ion mode, CID and subsequent reaction with water suggested that the strength of uranyl–neutral AA interactions follows the order His > Asp > Cys > Gly, which parallels the amino acid proton affinities. In negative ion mode, CID of $[UO_2(AA\text{-}H)_2(AA'\text{-}H)]^-$ and $[UO_2(AA\text{-}H)(AA'\text{-}H)_2]^-$ revealed decreasing dissociation in the order Gly >> His ≈ Cys > Asp, which presumably reflects enhanced binding of doubly deprotonated amino acids to uranyl in the reverse order.

Understanding the interactions of uranyl ions with biomolecules is essential in environmental/radiological protection and toxicology. Gas-phase ion chemistry experiments such as those described herein, involving amino acids as elementary components of peptides and proteins, can provide qualitative information on the basic properties of key species. They may serve as a foundation for more elaborate studies addressing structure and energetics, using spectroscopic and computational techniques, and can be especially relevant when radioactive species are involved.

Supplementary Materials: The following supporting information can be downloaded at https://www.mdpi.com/article/10.3390/app13063834/s1, Additional ESI and CID mass spectra obtained in the study; schemes with structures of the studied amino acids; tables with summaries of ESI-MS results; tables with gas-phase and solution data for the studied amino acids.

Author Contributions: A.F.L. and L.M. conducted the experiments and analyzed the results; J.K.G. and J.M. conceived and designed the study; A.F.L. wrote the original draft; L.M., J.K.G., and J.M. reviewed and edited the manuscript. All authors have read and agreed to the published version of the manuscript.

Funding: This work was supported by Fundação para a Ciência e a Tecnologia (FCT) through projects UIDB/00100/2020 (CQE) and LA/P/0056/2020 (IMS), and through RNEM—Portuguese Mass Spectrometry Network, ref. LISBOA-01-0145-FEDER-022125, also supported by the Lisboa Regional Operational Program (Lisboa2020), under the PT2020 Partnership Agreement, via the European Regional Development Fund (ERDF). FCT is also acknowledged for grant SFRH/BD/70475/2010 to A.F.L. and contract IST-ID/091/2018 to L.M. J.K.G. gratefully acknowledges support from the U.S. Department of Energy, Office of Science, Office of Basic Energy Sciences, Chemical Sciences, Geosciences, and Biosciences Division, Heavy Element Chemistry Program at the Lawrence Berkeley National Laboratory under contract DE-AC02-05CH11231.

Institutional Review Board Statement: Not applicable.

Informed Consent Statement: Not applicable.

Data Availability Statement: Data is contained within the article or supplementary material.

Conflicts of Interest: There are no conflicts of interest to report.

References

1. Ma, M.; Wang, R.; Xu, L.; Xu, M.; Liu, S. Emerging health risks and underlying toxicological mechanisms of uranium contamination: Lessons from the past two decades. *Environ. Int.* **2020**, *145*, 106107. [CrossRef] [PubMed]
2. Garai, A.; Delangle, P. Recent advances in uranyl binding in proteins thanks to biomimetic peptides. *J. Inorg. Biochem.* **2020**, *203*, 110936. [CrossRef]
3. Lin, Y.-W. Uranyl Binding to Proteins and Structural-Functional Impacts. *Biomolecules* **2020**, *10*, 457. [CrossRef] [PubMed]
4. Creff, G.; Zurita, C.; Jeanson, A.; Carle, G.; Vidaud, C.; Auwer, C.D. What do we know about actinides-proteins interactions? *Radiochim. Acta* **2019**, *107*, 993–1009. [CrossRef]
5. Carugo, O. Structural features of uranium-protein complexes. *J. Inorg. Biochem.* **2018**, *189*, 1–6. [CrossRef]
6. Pardoux, R.; Sauge-Merle, S.; Bremond, N.; Beccia, M.R.; Lemaire, D.; Battesti, C.; Delangle, P.; Solari, P.L.; Guilbaud, P.; Berthomieu, C. Optimized Coordination of Uranyl in Engineered Calmodulin Site 1 Provides a Subnanomolar Affinity for Uranyl and a Strong Uranyl versus Calcium Selectivity. *Inorg. Chem.* **2022**, *61*, 20480–20492. [CrossRef] [PubMed]
7. Starck, M.; Laporte, F.A.; Oros, S.; Sisommay, N.; Gathu, V.; Solari, P.L.; Creff, G.; Roques, J.; Auwer, C.D.; Lebrun, C.; et al. Cyclic Phosphopeptides to Rationalize the Role of Phosphoamino Acids in Uranyl Binding to Biological Targets. *Chem.—A Eur. J.* **2017**, *23*, 5281–5290. [CrossRef]
8. Qi, L.; Basset, C.; Averseng, O.; Quéméneur, E.; Hagège, A.; Vidaud, C. Characterization of UO_2^{2+}binding to osteopontin, a highly phosphorylated protein: Insights into potential mechanisms of uranyl accumulation in bones. *Metallomics* **2014**, *6*, 166–176. [CrossRef]
9. Deblonde, G.J.-P.; Sturzbecher-Hoehne, M.; Mason, A.B.; Abergel, R.J. Receptor recognition of transferrin bound to lanthanides and actinides: A discriminating step in cellular acquisition of f-block metals. *Metallomics* **2013**, *5*, 619–626. [CrossRef]
10. Götzke, L.; Schaper, G.; März, J.; Kaden, P.; Huittinen, N.; Stumpf, T.; Kammerlander, K.K.; Brunner, E.; Hahn, P.; Mehnert, A.; et al. Coordination chemistry of f-block metal ions with ligands bearing bio-relevant functional groups. *Coord. Chem. Rev.* **2019**, *386*, 267–309. [CrossRef]
11. Berto, S.; Crea, F.; Daniele, P.G.; Gianguzza, A.; Pettignano, A.; Sammartano, S. Advances in the investigation of dioxouranium(VI) complexes of interest for natural fluids. *Coord. Chem. Rev.* **2012**, *256*, 63–81. [CrossRef]
12. Bresson, C.; Ansoborlo, E.; Vidaud, C. Radionuclide speciation: A key point in the field of nuclear toxicology studies. *J. Anal. At. Spectrom.* **2011**, *26*, 593–601. [CrossRef]
13. Van Horn, J.D.; Huang, H. Uranium(VI) bio-coordination chemistry from biochemical, solution and protein structural data. *Coord. Chem. Rev.* **2006**, *250*, 765–775. [CrossRef]
14. Fattal, E.; Tsapis, N.; Phan, G. Novel drug delivery systems for actinides (uranium and plutonium) decontamination agents. *Adv. Drug Deliv. Rev.* **2015**, *90*, 40–54. [CrossRef]
15. Sturzbecher-Hoehne, M.; Deblonde, G.J.-P.; Abergel, R.J. Solution thermodynamic evaluation of hydroxypyridinonate chelators 3,4,3-LI(1,2-HOPO) and 5-LIO(Me-3,2-HOPO) for UO_2(VI) and Th(IV) decorporation. *Radiochim. Acta* **2013**, *101*, 359–366. [CrossRef]
16. Durbin, P.W.; Lauriston, S. Taylor lecture: The quest for therapeutic actinide chelators. *Health Phys.* **2008**, *95*, 465–492. [CrossRef] [PubMed]
17. Gorden, A.E.V.; Xu, J.; Raymond, K.N.; Durbin, P. Rational Design of Sequestering Agents for Plutonium and Other Actinides. *Chem. Rev.* **2003**, *103*, 4207–4282. [CrossRef]

18. Zhang, L.; Jia, M.; Wang, X.; Gao, L.; Zhang, B.; Wang, L.; Kong, J.; Li, L. A novel fluorescence sensor for uranyl ion detection based on a dansyl-modified peptide. *Spectrochim. Acta Part A Mol. Biomol. Spectrosc.* **2023**, *292*, 122403. [CrossRef]
19. Wu, X.; Huang, Q.; Mao, Y.; Wang, X.; Wang, Y.; Hu, Q.; Wang, H.; Wang, X. Sensors for determination of uranium: A review. *TrAC Trends Anal. Chem.* **2019**, *118*, 89–111. [CrossRef]
20. Safi, S.; Jeanson, A.; Roques, J.; Solari, P.L.; Charnay-Pouget, F.; Auwer, C.D.; Creff, G.; Aitken, D.J.; Simoni, E. Thermodynamic and Structural Investigation of Synthetic Actinide–Peptide Scaffolds. *Inorg. Chem.* **2016**, *55*, 877–886. [CrossRef]
21. Zhou, L.; Bosscher, M.; Zhang, C.; Özçubukçu, S.; Zhang, L.; Zhang, W.; Li, C.J.; Liu, J.; Jensen, M.P.; Lai, L.; et al. A protein engineered to bind uranyl selectively and with femtomolar affinity. *Nat. Chem.* **2014**, *6*, 236–241. [CrossRef] [PubMed]
22. Odoh, S.O.; Bondarevsky, G.D.; Karpus, J.; Cui, Q.; He, C.; Spezia, R.; Gagliardi, L. UO_2^{2+} Uptake by Proteins: Understanding the Binding Features of the Super Uranyl Binding Protein and Design of a Protein with Higher Affinity. *J. Am. Chem. Soc.* **2014**, *136*, 17484–17494. [CrossRef]
23. Lebrun, C.; Starck, M.; Gathu, V.; Chenavier, Y.; Delangle, P. Engineering Short Peptide Sequences for Uranyl Binding. *Chem.—A Eur. J.* **2014**, *20*, 16566–16573. [CrossRef] [PubMed]
24. Carlton, D.D.; Schug, K.A. A review on the interrogation of peptide–metal interactions using electrospray ionization-mass spectrometry. *Anal. Chim. Acta* **2011**, *686*, 19–39. [CrossRef]
25. Rodgers, M.T.; Armentrout, P.B. A Thermodynamic "Vocabulary" for Metal Ion Interactions in Biological Systems. *Acc. Chem. Res.* **2004**, *37*, 989–998. [CrossRef]
26. Rodgers, M.T.; Armentrout, P.B. Cationic Noncovalent Interactions: Energetics and Periodic Trends. *Chem. Rev.* **2016**, *116*, 5642–5687. [CrossRef] [PubMed]
27. Polfer, N.C.; Oomens, J. Vibrational spectroscopy of bare and solvated ionic complexes of biological relevance. *Mass Spectrom. Rev.* **2009**, *28*, 468–494. [CrossRef]
28. Dunbar, R.C. Spectroscopy of Metal-Ion Complexes with Peptide-Related Ligands. In *Gas-Phase IR Spectroscopy and Structure of Biological Molecules*; Rijs, A., Oomens, J., Eds.; Topics in Current Chemistry; Springer: Cham, Switzerland, 2015; Volume 364, pp. 183–223. [CrossRef]
29. Jašíková, L.; Roithová, J. Infrared Multiphoton Dissociation Spectroscopy with Free-Electron Lasers: On the Road from Small Molecules to Biomolecules. *Chem.—A Eur. J.* **2018**, *24*, 3374–3390. [CrossRef]
30. Jones, R.M.; Nilsson, T.; Walker, S.; Armentrout, P.B. Potassium Binding Interactions with Aliphatic Amino Acids: Thermodynamic and Entropic Effects Analyzed via a Guided Ion Beam and Computational Study. *J. Am. Soc. Mass Spectrom.* **2022**, *33*, 1427–1442. [CrossRef]
31. IAEA Live Chart of Nuclides. Available online: https://www-nds.iaea.org/relnsd/vcharthtml/VChartHTML.html (accessed on 26 February 2023).
32. Jones, C.M.; Bernier, M.; Carson, E.; Colyer, K.E.; Metz, R.; Pawlow, A.; Wischow, E.D.; Webb, I.; Andriole, E.J.; Poutsma, J.C. Gas-phase acidities of the 20 protein amino acids. *Int. J. Mass Spectrom.* **2007**, *267*, 54–62. [CrossRef]
33. Smith, J.R.; Kim, J.B.; Lineberger, W.C. High-resolution threshold photodetachment spectroscopy of OH^-. *Phys. Rev. A* **1997**, *55*, 2036–2043. [CrossRef]
34. Di Marco, V.B.; Bombi, G.G. Electrospray mass spectrometry (ESI-MS) in the study of metal–ligand solution equilibria. *Mass Spectrom. Rev.* **2006**, *25*, 347–379. [CrossRef] [PubMed]
35. Tsierkezos, N.G.; Roithová, J.; Schröder, D.; Ončák, M.; Slavíček, P. Can Electrospray Mass Spectrometry Quantitatively Probe Speciation? Hydrolysis of Uranyl Nitrate Studied by Gas-Phase Methods. *Inorg. Chem.* **2009**, *48*, 6287–6296. [CrossRef]
36. Keith-Roach, M.J. A review of recent trends in electrospray ionisation–mass spectrometry for the analysis of metal–organic ligand complexes. *Anal. Chim. Acta* **2010**, *678*, 140–148. [CrossRef] [PubMed]
37. Indelicato, S.; Bongiorno, D.; Ceraulo, L. Recent Approaches for Chemical Speciation and Analysis by Electrospray Ionization (ESI) Mass Spectrometry. *Front. Chem.* **2021**, *8*, 625945. [CrossRef] [PubMed]
38. Haynes, W.M.; Lide, D.R.; Bruno, T.J. (Eds.) *CRC Handbook of Chemistry and Physics*, 97th ed.; CRC Press: Boca Raton, FL, USA, 2017.
39. Groenewold, G.S.; de Jong, W.A.; Oomens, J.; Van Stipdonk, M.J. Variable denticity in carboxylate binding to the uranyl coordination complexes. *J. Am. Soc. Mass Spectrom.* **2010**, *21*, 719–727. [CrossRef] [PubMed]
40. Dookeran, N.N.; Yalcin, T.; Harrison, A.G. Fragmentation Reactions of Protonated α-Amino Acids. *J. Mass Spectrom.* **1996**, *31*, 500–508. [CrossRef]
41. Rogalewicz, F.; Hoppilliard, Y.; Ohanessian, G. Fragmentation mechanisms of α-amino acids protonated under electrospray ionization: A collisional activation and ab initio theoretical study. *Int. J. Mass Spectrom.* **2000**, *195–196*, 565–590. [CrossRef]
42. Zhang, P.; Chan, W.; Ang, I.L.; Wei, R.; Lam, M.M.T.; Lei, K.M.K.; Poon, T.C.W. Revisiting Fragmentation Reactions of Protonated α-Amino Acids by High-Resolution Electrospray Ionization Tandem Mass Spectrometry with Collision-Induced Dissociation. *Sci. Rep.* **2019**, *9*, 6453. [CrossRef]
43. Armentrout, P.B. Energetics and mechanisms for decomposition of cationized amino acids and peptides explored using guided ion beam tandem mass spectrometry. *Mass Spectrom. Rev.* **2021**, 1–26. [CrossRef]
44. O'Hair, R.A.J.; Rijs, N.J. Gas Phase Studies of the Pesci Decarboxylation Reaction: Synthesis, Structure, and Unimolecular and Bimolecular Reactivity of Organometallic Ions. *Acc. Chem. Res.* **2015**, *48*, 329–340. [CrossRef] [PubMed]

45. Dau, P.D.; Rios, D.; Gong, Y.; Michelini, M.C.; Marçalo, J.; Shuh, D.K.; Mogannam, M.; Van Stipdonk, M.J.; Corcovilos, T.A.; Martens, J.K.; et al. Synthesis and Hydrolysis of Uranyl, Neptunyl, and Plutonyl Gas-Phase Complexes Exhibiting Discrete Actinide–Carbon Bonds. *Organometallics* **2016**, *35*, 1228–1240. [CrossRef]
46. van Stipdonk, M.J.; Tatosian, I.J.; Iacovino, A.C.; Bubas, A.R.; Metzler, L.J.; Sherman, M.C.; Somogyi, A. Gas-Phase Deconstruction of UO_2^{2+}: Mass Spectrometry Evidence for Generation of $[OU^{VI}CH]^+$ by Collision-Induced Dissociation of $[U^{VI}O_2(C{\equiv}CH)]^+$. *J. Am. Soc. Mass Spectrom.* **2019**, *30*, 796–805. [CrossRef] [PubMed]
47. Xiong, Z.; Chen, X.; Gong, Y. Mass spectrometric and theoretical study on the formation of uranyl hydride from uranyl carboxylate. *Phys. Chem. Chem. Phys.* **2021**, *23*, 20073–20079. [CrossRef] [PubMed]
48. Lucena, A.F.; Carretas, J.M.; Marçalo, J.; Michelini, M.C.; Gong, Y.; Gibson, J.K. Gas-Phase Reactions of Molecular Oxygen with Uranyl(V) Anionic Complexes—Synthesis and Characterization of New Superoxides of Uranyl(VI). *J. Phys. Chem. A* **2015**, *119*, 3628–3635. [CrossRef]
49. Groenewold, G.S.; Cossel, K.C.; Gresham, G.L.; Gianotto, A.K.; Appelhans, A.D.; Olson, J.E.; Van Stipdonk, M.J.; Chien, W. Binding of Molecular O_2 to Di- and Triligated $[UO_2]^+$. *J. Am. Chem. Soc.* **2006**, *128*, 3075–3084. [CrossRef]
50. Bryantsev, V.S.; de Jong, W.A.; Cossel, K.C.; Diallo, M.S.; Goddard, I.W.A.; Groenewold, G.S.; Chien, W.; Van Stipdonk, M.J. Two-Electron Three-Centered Bond in Side-On (η2) Uranyl(V) Superoxo Complexes. *J. Phys. Chem. A* **2008**, *112*, 5777–5780. [CrossRef]
51. Leavitt, C.M.; Bryantsev, V.S.; de Jong, W.A.; Diallo, M.S.; Iii, W.A.G.; Groenewold, G.S.; Van Stipdonk, M.J. Addition of H_2O and O_2 to Acetone and Dimethylsulfoxide Ligated Uranyl(V) Dioxocations. *J. Phys. Chem. A* **2009**, *113*, 2350–2358. [CrossRef]
52. Rios, D.; Michelini, M.C.; Lucena, A.F.; Marçalo, J.; Bray, T.H.; Gibson, J.K. Gas-Phase Uranyl, Neptunyl, and Plutonyl: Hydration and Oxidation Studied by Experiment and Theory. *Inorg. Chem.* **2012**, *51*, 6603–6614. [CrossRef]
53. Hunter, E.P.L.; Lias, S.G. Evaluated Gas Phase Basicities and Proton Affinities of Molecules: An Update. *J. Phys. Chem. Ref. Data* **1998**, *27*, 413–656. [CrossRef]